Exchange bias in ferrite hollow nanoparticles originated by complex internal magnetic structure

2015 Mater. Res. Express 2 105001

(http://iopscience.iop.org/2053-1591/2/10/105001)

Materials Research Express

PAPER

Exchange bias in ferrite hollow nanoparticles originated by complex internal magnetic structure

RECEIVED
28 July 2015

REVISED
27 August 2015

ACCEPTED FOR PUBLICATION
10 September 2015

PUBLISHED
5 October 2015

Emilio De Biasi[1], Enio Lima Jr[1], Jose M Vargas[1], Roberto D Zysler[1], Jordi Arbiol[2], Alfonso Ibarra[3], Gerardo F Goya[3] and M Ricardo Ibarra[3]

[1] Centro Atómico Bariloche/CONICET, 8400 SC de Bariloche, RN, Argentina
[2] GAEN-CeMARC, Group of Advanced Electron Nanoscopy—Centre de Microscopia d'Alta Resolució de Catalunya, Universitat de Barcelona, E-08028 Barcelona, Spain
[3] Instituto de Nanociencia de Aragón, Universidad de Zaragoza, E-50009 Zaragoza, Spain

E-mail: debiasi@cab.cnea.gov.ar

Keywords: nanomagnetism, micromagnetism, nanoparticles

Abstract

Iron-oxide hollow nanospheres (HNS) may present unusual magnetic behavior as a consequence of their unique morphology. Here, we report the unusual magnetic behavior of HNS that are 9 nm in diameter. The magnetic properties of HNS originate in their complex magnetic structure, as evidenced by Mössbauer spectroscopy and magnetization measurements. We observe a bias in the hysteresis when measured at very low temperature in the field cooling protocol (10 kOe). In addition, dc (static) and ac (dynamic) magnetization measurements against temperature and applied field reveal a frustrated order of the system below 10 K. High-resolution transmission electron microscopy (HRTEM) studies reveal that the HNS are composed of small crystalline clusters of about 2 nm in diameter, which behave as individual magnetic entities. Micromagnetic simulations (using conjugate gradient in order to minimize the total energy of the system) reproduce the experimentally observed magnetic behavior. The model considers the hollow particles as constituted by small ordered clusters embedded in an antiferromagnetic environment (spins localized outside the clusters). In addition, the surface spins (in both inner and outer surfaces of the HNS) are affected by a local surface anisotropy. The strong effective magnetic anisotropy field of the clusters induces the bias observed when the system is cooled in the presence of a magnetic external field. This effect propagates through the exchange interaction into the entire particle.

1. Introduction

A finite size-effect occurs in nanostructured materials such as thin films, nanoparticles (NPs) and nanowires [1]. The control of their morphology and functionalities at the nanoscale leads to unique magnetic properties, and they are prerequisites for several applications, such as nanovectors for drug delivery [2, 3]. In particular, spherical empty nanocapsules are appealing for this latter application because they can store larger amounts of drug in comparison to the respective solid NPs [4–6].

The magnetic behavior of nanostructures is strongly influenced by the surface effects, since the magnetic behavior of the surface atoms is characterized by a lack of symmetry and broken exchange bonds, which introduce structural and magnetic disorder and originate an enhancement of the magnetic anisotropy and the coercive field [7]. On the basis of their huge surface/bulk atomic ratio, magnetic hollow nanospheres (HNS) provide an excellent scenario to study the competition between the magnetic responses of the surface and core at the nanoscale level, opening up new perspectives for theoretical developments. The unique magnetic phenomena reported for magnetic nanoparticles in the last several years have usually been assigned to the complex surface microstructure and/or exchange interactions at the core/surface interface [8, 9]. Our group have reported on the synthesis of iron-oxide HNS with unusual magnetic behavior [10], specifically a high exchange bias field (H) at low temperature in field-cooling mode (defined as $H_B = |H_C^+ + H_C^-/2|$, where H_C^+

and H_C^- are the positive and negative coercive field, respectively). In this reference [10], preliminary analyses of the morphology of the HNS with High-Resolution Transmission Electron Microscopy (HRTEM) indicate an internal structure with the presence of small crystals.

In this work we have studied in detail the anomalous magnetic properties of the HNS system whose synthesis was reported previously [10], and we interpret these results with simulations obtained from a micromagnetic model. Experimentally, the most relevant feature observed is the bias of the hysteresis loops at low temperature, when the sample is cooled under the presence of an external magnetic field. According to the micromagnetic model, the strong anisotropy field of the internal clusters generates an effective field which propagates its influence over all spins of the particle through the exchange interaction. The micromagnetic simulations also show that the surface anisotropy plays an important role when its value is close to or lower than the effective anisotropy field, favoring the increase of the exchange bias.

2. Sample preparation and morphological characterization:

Production of the 9.3 nm diameter hollow nanospheres is described in a previous article [10]. Briefly, hollow nanospheres were prepared by the high temperature (543 K) decomposition of $Fe(acac)_3$ (iron(III) acetylacetonate) in the presence of 1, 2-hexadecanediol (a long-chain alcohol), oleic acid and oleylamine, with the synthesis procedure started at the reflux condition (543 K) in argon flux ($\sim$0.5 cm^3 min^{-1}). After $\sim$5 min the temperature was cooled down to 473 K over 30 min. The final particles were coated with a hydrophobic organic layer. For magnetic and Mössbauer measurements, the HNS were conditioned by dispersing them in a polymeric matrix (PEI) in a concentration of 0.5 % wt., reducing the interparticle interactions.

The hollow nature of the nanoparticles was previously demonstrated by different techniques based on TEM analysis [10]. Here, in order to determine the effect of morphology on the magnetic properties of the system, we make a new morphological characterization of the HNS. For this, the particles were dispersed in an organic solvent and dropped onto a copper grid with an ultrathin carbon coating. The sample was analyzed with High-resolution TEM (HRTEM) combined with Energy Electron Loss Spectroscopy (EELS), Energy Filtered TEM (EFTEM) and high angular annular dark field (HAADF). Figure 1(a) shows a general view of the sample where 9.3 nm diameter nanoparticles are observed, and the hollow structure of all particles is indicated. The HAADF image presented in figure 1(b) indicates the presence of a crystalline phase with the interplanar distance expected for the ferrite structure (not shown), similar to that observed previously [10]. The HAADF profile of one nanoparticle, shown in figure 1(c) (dashed line), confirms the hollow nature of the structure, which is well-fitted with a model of a hollow particle (solid line). EELS and EFTEM analysis (not shown) have revealed that the only elements composing the nanospheres were Fe and O. Finally, detailed analysis using magnified HRTEM (figure 1(d)) reinforces the polycrystalline nature of the nanostructures, which are composed of crystallites of 2 nm in size.

3. Magnetic characterizations

In the previous work published on the HNS [10], Mössbauer spectra of the HNS taken at 300 K gave a superparamagnetic doublet with Fe^{3+} signature and reflecting a local symmetry lower than cubic, implying broken Fe–Fe superexchange paths and/or oxygen vacancies at high temperature. At 4.2 K, the spectrum presents two sub-lattices (two sextets) with lower hyperfine field B_{hyp} than expected for A and B sites of ferrite. Here, in order to investigate in detail the magnetic structure of the HNS, we present in figure 2(a) the in-field Mössbauer spectrum taken at 4.2 K with applied field of 120 kOe in field-cooling mode, starting at room temperature. For comparison, the Mössbauer spectrum measured in a similar setup of a crystalline 5 nm ferrite nanoparticle is given in figure 2(b). These spectra were collected in a liquid He flow cryostat with a conventional constant-acceleration spectrometer in transmission geometry using a $^{57}Co/Rh$ source. The samples are prepared between acrylic discs and mounted in the bore of a 140 kOe superconducting magnet, in a vertical source-sample-detector setup such that the direction of gamma-ray propagation is parallel to the applied magnetic field axis. Both spectra are fitted using Lorentzian line shapes with a non-linear least-squares program, calibrating the velocity scale with a foil of α-Fe at 300 K, and a distribution of hyperfine fields and isomer shift have been used to fit the spectrum of the HNS sample. The Mössbauer spectrum of the HNS is fitted with two crystallite sites referent to sites A and B (effective hyperfine field $B_{eff} = B_{hyp} + B_{app} = 612$ kOe and 389 kOe, respectively, and a total relative absorption area of 13%) and a broad hyperfine field distribution (inset of figure 2(a)), with similar distribution in the hyperfine field from 400 kOe to 600 kOe. In counterpart, the in-field Mössbauer spectrum of the crystalline 5 nm ferrite nanoparticle exhibits the two sextets, which are associated to sites A and B of the ferrite. The strong reduction observed for the absorption of lines 2 and 5 in both magnetic sub-lattices indicates that they are aligned with the direction of the applied field. Spin canting can be directly

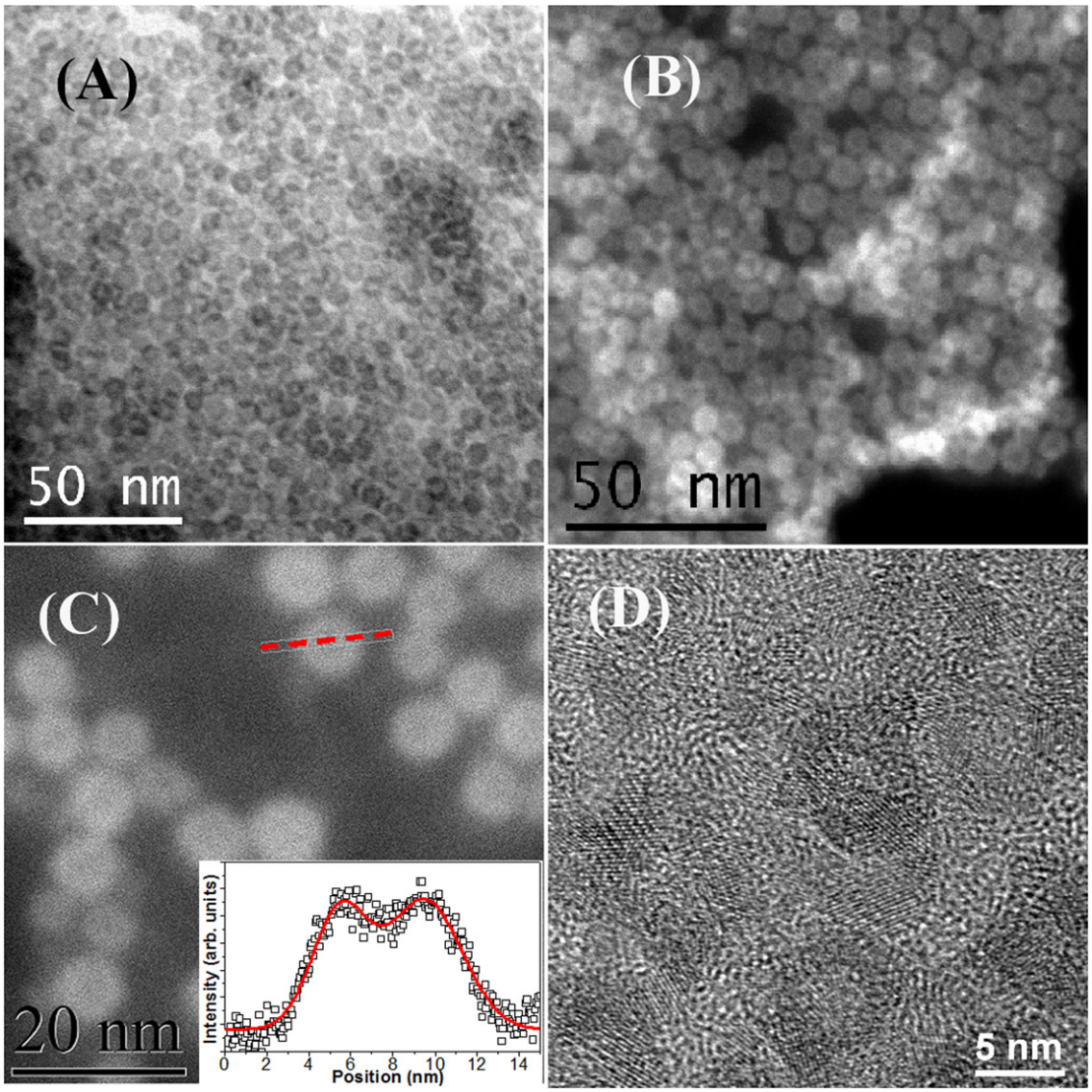

Figure 1. (A) Representative TEM micrograph of the HNS, (B) representative dark field image of the HNS, (C) representative HAADF-STEM image of the HNS and (D) representative HRTEM micrograph of the HNS. The inset shows a STEM profile through one single nanoparticle, indicated by the dashed line in (D).

evidenced by in-field Mössbauer spectroscopy, being distinguished from the paramagnetism at low temperatures due to the presence of the MS spectra, which splits magnetically with an incomplete polarization at high applied fields [11] (broad hyperfine field distributions). In this way, the spins in the crystalline 5 nm ferrite nanoparticle are almost completely ordered, while the broad hyperfine field distribution in the HNS spectrum can be addressed to a large quantity of disordered (87%) and frozen spins, even for an applied field as large as 120 kOe.

Figure 3 displays the M(T) curves (H = 20 Oe) measured in the ZFC and FC (cooling field H = 20 Oe) modes. The ZFC results exhibit a sharp peak at ~40 K. This temperature coincides with the irreversibility temperature (i.e. the temperature above which the ZFC and FC curves merge). This indicates the existence of a very narrow energy barrier distribution, reflecting a narrow size dispersion, as observed in figure 1(a). The inset of figure 3 displays the out-of-phase component χ'' of ac susceptibility as a function of temperature under a magnetic field of 2 Oe and at frequencies $f = 0.5, 1, 3$ and 10 kHz. The results exhibit two maxima located at $T_B = 40$–48 K and $T_f \sim 11$ K. The maximum at T_B was associated to the blocking process of the superparamagnetic (SPM) magnetic moments in the inner part of the particle body, hereafter (BULK). T_B has a large dependence on frequency, which is an indication of the existence of a thermally activated mechanism, with an energy barrier $E_a = 1.8 \times 10^{-13}$ *erg*, as expected for the blocking process in the Néel-Brown model [12, 13]. The second maximum at T_f (lower temperatures than T_B) hardly changes at all with frequency. On the other hand, the ZFC curve exhibits a minimum at approximately 18 K, and the magnetization increases suddenly at low temperatures, as happen with the FC curve. These types of features are typical of attempts to reach magnetic

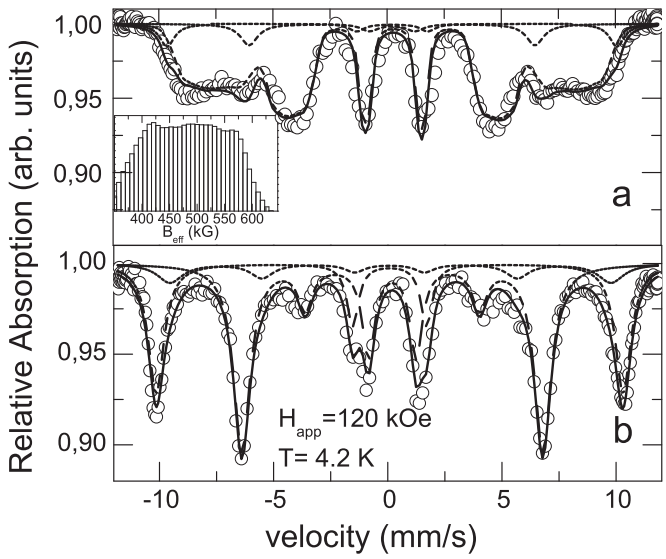

Figure 2. Mössbauer spectra of (a) HNS and (b) crystalline 5 nm ferrite nanoparticles collected at 4.2 K with applied field of $H_{app} = 120$ kOe. Inset of Figure (a): hyperfine field distribution obtained from the fitting.

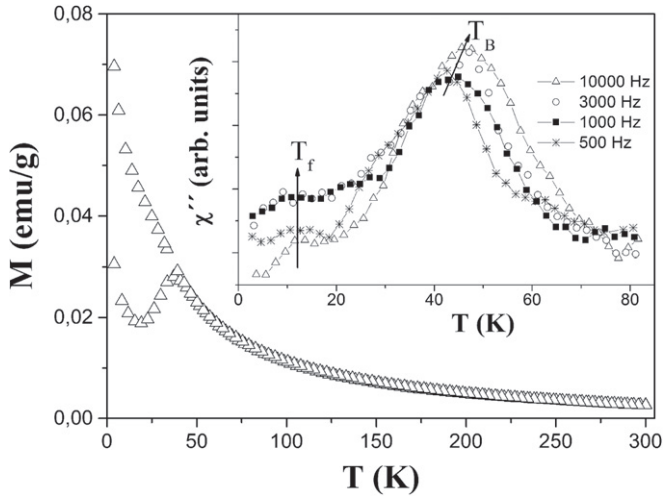

Figure 3. ZFC (lower branch) and FC (upper branch) magnetization curves as a function of the temperature (from 2 K up to 300 K) with applied field of $H = 20$ Oe. Inset: thermal and frequency dependence of the out-of-phase χ'' component of the ac susceptibility.

ordering at low temperatures [14–17]. Considering the experimental evidence, we can assert that there are at least two contributions to the magnetization. First, there are magnetic ordered regions, probably associated to the structural ordered region of the particles (i.e. the 2 nm clusters observed in HRTEM studies), which contribute to the observed 40 K maximum on ZFC (dependence with measuring frequency in ac susceptibility): the blocking temperature. The second contribution comes from a substantial fraction of magnetically disordered spins of the particle, which tends to be ordered at low temperature. This produces an increase in the magnetization; however at low temperatures the system frustrates. This interpretation is also consistent with the in-field Mössbauer observation, that it is supporting a large fraction of disordered spins (87%).

Figure 4 presents the hysteresis loops measured at 2 K in ZFC (M_{ZFC}) and FC (M_{FC}) protocols with an external applied field of $H = 10$ kOe. The figure is split into four: panel (A) shows a general landscape of the hysteresis loops, (B) gives a zoom on the low field region and a small inset showing the Exchange Field (H_B) as a function of temperature; panels (C) and (D) show a zoom of the high field regions. Panel (A) demonstrates that the magnetization cannot achieve the saturation and has a smooth curvature. In addition, a vertical shift of the FC hysteresis loop is observed, especially at high positive values of *H*. Panels (C) and (D) confirm the last observation, showing the $M_{FC}(H)$ curve above the $M_{ZFC}(H)$ one. The principal feature is detailed in panel (B) of figure 4. The horizontal bias of the FC measurement, which is not observed in the ZFC case, is noticeable.

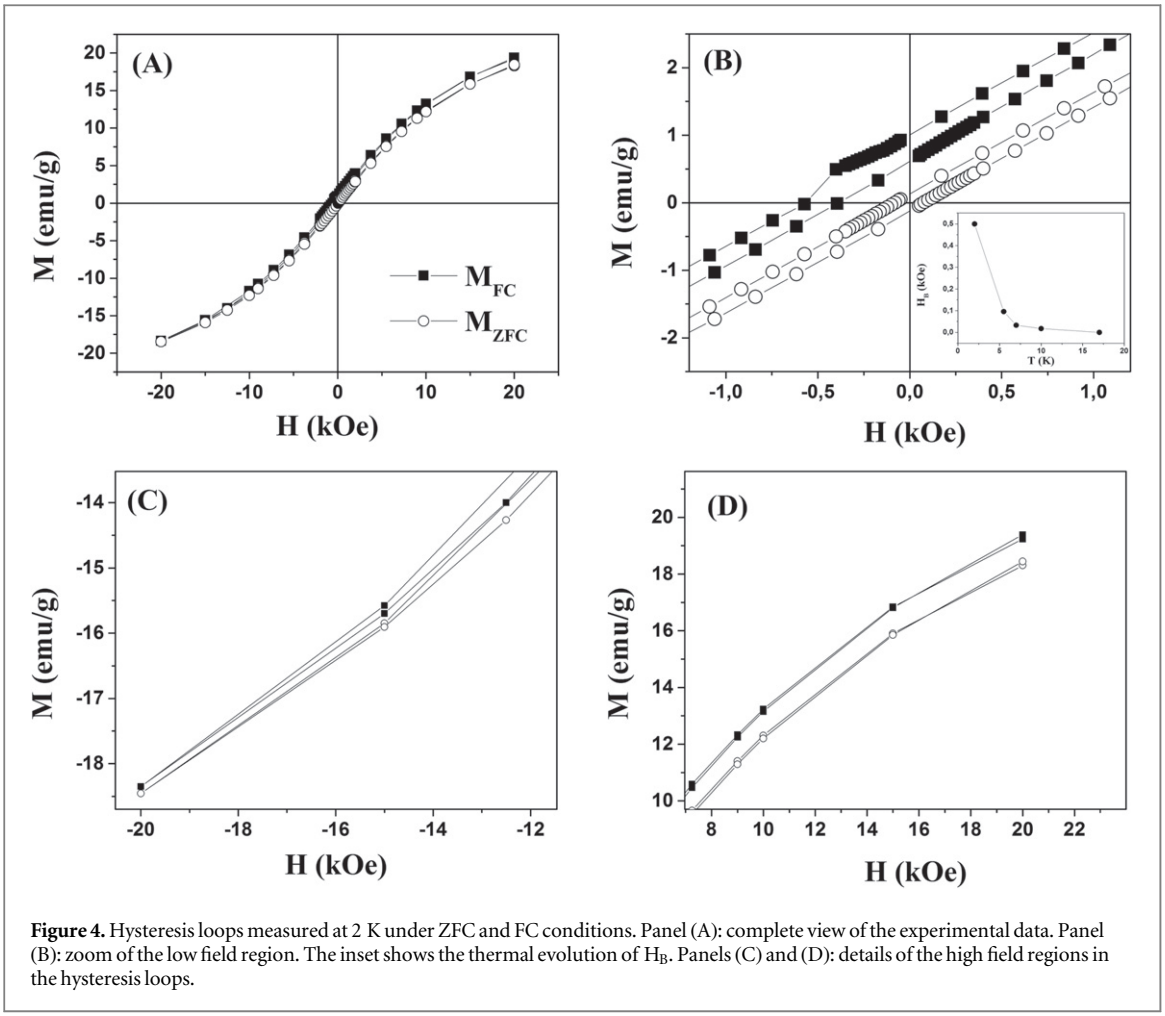

Figure 4. Hysteresis loops measured at 2 K under ZFC and FC conditions. Panel (A): complete view of the experimental data. Panel (B): zoom of the low field region. The inset shows the thermal evolution of H_B. Panels (C) and (D): details of the high field regions in the hysteresis loops.

There is a small coercive field (H_C). However, the value of the irreversibility field is larger than the value of H_C. The inset of panel (B) shows the exchange field (H_B) evolution as a function of the temperature; this vanishes at temperatures above 20 K and, on the other hand, exhibits a strong increment below 6 K. The observed features can be understood using the information disclosed previously: TEM images (figure 1), Mössbauer spectroscopy (figure 2) and M(T) and χ'' curves (figure 3).

The exchange bias behavior observed in the $M_{FC}(H)$ hysteresis loop is dominated by the internal magnetic cluster dynamics of each particle. Below 18 K, the magnetic order of these clusters grows because the exchange interaction starts to overcome the effect of the thermal fluctuations, and they cannot reverse their magnetization easily. This effect increases both the magnetization of the particle and the internal effective field generated by the internal clusters, and propagates inside the particle. This field is responsible for the observed bias in the FC case. As the temperature diminishes, this effect becomes more important, and the exchange bias increases. In the ZFC case, the magnetization of the clusters points 'randomly,' and then the average internal effective field result is null.

As the temperature is lowered, the ordering of the spins makes the surface anisotropy of the particle become more important [15, 17]. This fact induces a frustrated state in the magnetic behavior of the system, which is reflected in the maximum observed at T_f in figure 3. At ~6 K, the surface spins starts to get a local order, which induces an abrupt increase in the magnetization; this also helps to increase the exchange effective field.

4. Theory and simulations

In order to understand the microscopic spin process in the nanoparticle, we perform micromagnetic simulations. The focus of these calculations is to support our microscopic interpretation of the exchange bias origin, and to help us understand the role played by the surface anisotropy.

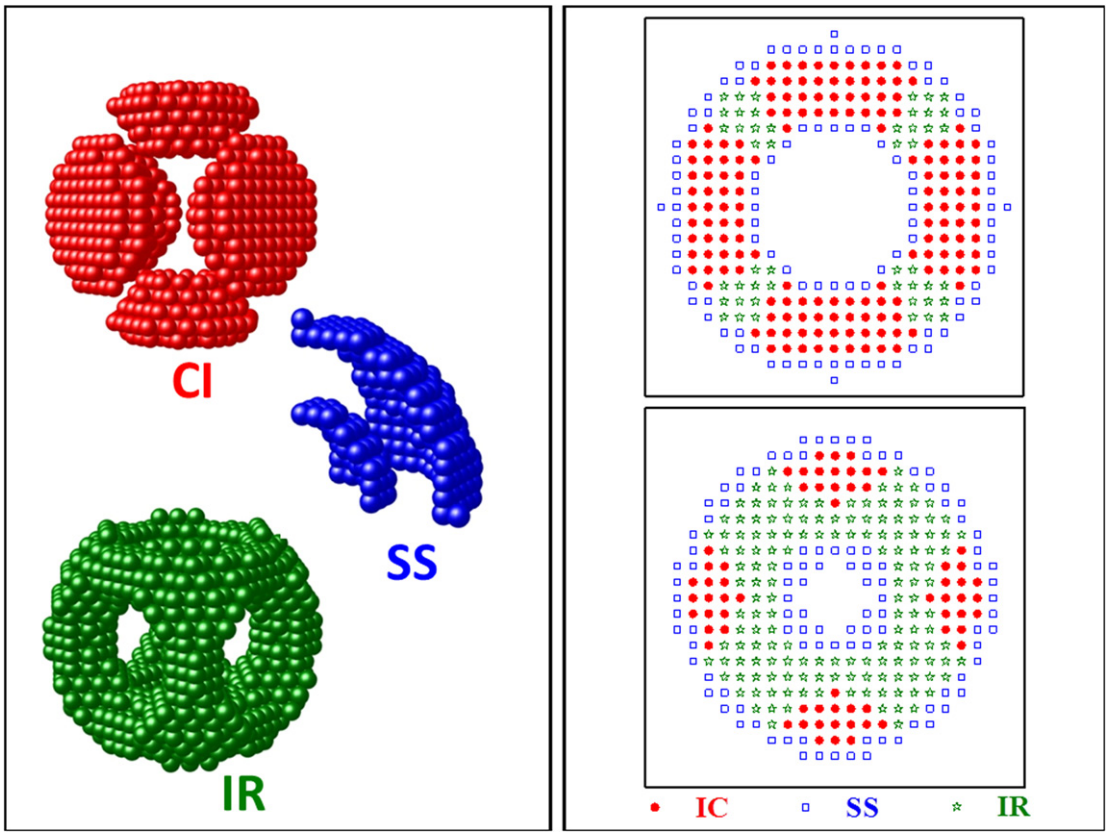

Figure 5. Left: Details of the particle construction. Right: upper panel shows a cross section through the center of the particle indicating the spatial distribution of the spins; lower panel is similar but this cross section is taken at four planes of distance from the center.

4.1. Micromagnetic model

The micromagnetic model used in this work is based on a hollow spherical particle, divided into three different regions: interstitial clusters of magnetic moments (IC), surface spins (SS), and spins associated to the so-called intermediate region (IR), which corresponds to the remaining magnetic moments between the IC. Figure 5 shows a diagram with each of the mentioned regions. In the model we refer either to spin or magnetic moments as the effective magnetic moment associated to the unit cell of the ferrite, which is around 4 μ_B [18]. The IC corresponds to the spins associated to the lattice sites favored by the local crystalline order, as revealed in the HRTEM studies. In our model, each IC is considered as a unique magnetic entity. There are six ICs symmetrically distributed in each axis of the model particle (see figure 5). The effective magnetic moment of the IC comes from the decompensation of the ferrimagnetic structure. The SS are located in the inner and outer surface regions. They are affected by the surface anisotropy, which comes from the break on the spin lattice symmetry due to the interface of the particle with the vacuum, and modify the coordination number of the surface sites. In general, all the spins not contained in the clusters are treated as individual entities. Figure 5 also shows a cross section through the center (upper panel on the right) and four planes of distance from the center (lower panel on the right) in which the topography is detailed, corresponding to the IC, SS, and IR spin regions.

The particle is composed of a total of 5186 spins, distributed as follows: 6 clusters of 292 spins, 350 and 1436 magnetic surface moment inner and outer spins of the surface, respectively, and 1648 spins of the intermediate region.

The total magnetic energy of the particle is composed of several contributions. In equation (1) we express the Hamiltonian of the system:

$$\mathcal{H} = -\sum_{i\ \mathrm{clus}} \vec{\mu}_{i\ \mathrm{clus}} \cdot \vec{H} - \sum_{i} \vec{\mu}_i \cdot \vec{H} - K_A \sum_{i\ \mathrm{clus}} \left(\hat{n}_i \cdot \hat{\mu}_{i\ \mathrm{clus}}\right)^2 - \tilde{K}_A \sum_{i} \left(\hat{n}_i \cdot \hat{\mu}_i\right)^2 + \\ - J \sum_{i \neq j} \hat{\mu}_i \cdot \hat{\mu}_j - K_{\mathrm{sup}} \sum_{i} \left(\hat{r}_i \cdot \hat{\mu}_{i\ \mathrm{sup}}\right)^2 \qquad (1)$$

The first and second term of equation (1) correspond to the Zeeman energy of the IC and the remaining spins of the particle, respectively. In these terms, $\vec{\mu}_i$ denotes the magnetic moment of each particular spin, and

$\vec{\mu}_{i\ clus}$ is associated to the IC. The third and fourth terms of equation (1) are associated to the magnetocrystalline energy of the clusters, and the others spin with anisotropy constant K_A y $\tilde{K}_A$, respectively. In our model we assume that the easy anisotropy axes are oriented along the direction defined by the external magnetic field. The value associated to K_A corresponds, approximately, to the bulk material (5×10^5 erg cm^{-3}), but in the case of the other spins we use a value one order of magnitude lower, in light of the fact that these spins do not correspond with sites in the material with a well-defined crystalline structure, as in the case of the IC.

The fifth term of $\mathcal{H}$ describes the antiferromagnetic exchange interaction between the spins. The value of the exchange constant J is associated to approximately 10 K, with the temperature of the spins assuming a mean field model [19]. The last term in equation (1) corresponds to the surface anisotropy, which is taking into account only the surface moments $\hat{\mu}_{i\ \mathrm{sup}}$. K_{sup} is the surface anisotropy constant. This constant, which was not previously determined from measurements, is a free parameter in the simulations. $\hat{r}_i$ is the unitary vector which indicates the orientation of the easy axis of surface anisotropy in each point of the particle. In this model it is assumed that the universal vector $\hat{r}_i$ points along the radial direction according to the position of the cell of the spin *i*.

The model, synthesized in equation (1), does not consider the effects due to the thermal fluctuations. These effects are not relevant in the simulation because we are interested in the simulation of hysteresis loops performed at 2 K (see figure 4). At this temperature the thermal energy is not relevant in reference to the energy contributions of equation (1).

The simulations were performed by minimizing the total magnetic energy for each value of the external magnetic field. When the local minimum was achieved, we calculated the magnetization corresponding to the spin configuration obtained. Due to the large complexity of the minimizing problem, which does not have an analytical solution, and the existence of large number of degrees of freedom, it is necessary to use numerical methods of optimization. In our case, we used the conjugate gradient methods, more precisely the Fletcher–Reeves algorithm [20, 21].

In the proposed model, we do not consider the effect of the magnetostatic energy term. There are several reasons for this exclusion. In first place of importance, we consider the small total magnetization of the system. This occurs not only by a small magnetic moment per cell, but also by the dominant antiferromagnetic order; the surface anisotropy also conspires against the magnetic order and the total magnetization of the particle. In addition, the spherical shape of the proposed particle model (which is consistent with the HRTEM observations) avoids the existence of preferential orientations of the magnetization. Second, in the size range for which the description is given (a few nanometers), the local magnetostatic energy is negligible compared to the other terms addressed in equation (1). In the same sense, due to the low effective magnetization, the interparticle interactions are not taken into account.

5. Results of the simulations

The simulations were performed considering two alternatives for the loop 'measurements.' The simulations consider both cases, in accordance with the experimental protocols, i.e. associated to the field cooling and zero field cooling magnetization measurement procedures. As we do not include thermal effects in the actual description, in order to consider the cases of M_{FC} and M_{ZFC}, we start the simulations from spin configurations compatible with each measurement protocol. In the case of M_{FC} simulations, all the spins are randomly initialized, with the exception of the cluster ones. In these cases the effective magnetic moment $\vec{\mu}_{i\ clus}$ is originally oriented along the external field direction. On the other hand, in the ZFC protocol, the simulations start from a spin configuration in which IC moments are randomly oriented. This choice for the initial spin configuration is based on the assumption that the clusters have an effective field anisotropy large enough to retain the magnetization configuration achieved by cooling the system. In the case of the ZFC protocol, the expected zero magnetization is simulated by a randomly oriented $\vec{\mu}_{i\ \mathrm{clus}}$ initialization. Conversely, in the FC case, we assume the $\vec{\mu}_{i\ \mathrm{clus}}$ is magnetized along the orientation of the external magnetic field. It is important to note that the other spins (SS, IR) are randomly initialized, assuming that the exchange interaction and surface anisotropy energy, as well as the thermal energy, contribute to demagnetize them. Considering these initial magnetic configurations chosen for the SS and IC spins, it is clear that they do not correspond to the ones that would reach the spin system by the effects of interparticle interactions. In order to solve this problem, and also to make a more realist description, we simulate the initial curve sweeping the magnetic field from zero up to Hmax (approximately corresponding to 1 Tesla in our simulations); the field is then swept until –Hmax and Hmax in order to perform the hysteresis loop simulation. This allows the system to reach a spin configuration at Hmax compatible with the intraparticle interactions. Each hysteresis loop is the result of the average of 30 statistically equivalent realizations.

Table 1. Numerical values of the parameters used in the micro-magnetic simulations.

Reduced Parameter	Value
$\mu^*_{i\ \mathrm{clus}}$	3.2×10^{-3}
μ^*_i	1.8×10^{-4}
K^*_A	1
$\tilde{K}^*_A$	0.1
J^*	0.8
K^*_{sup}	4

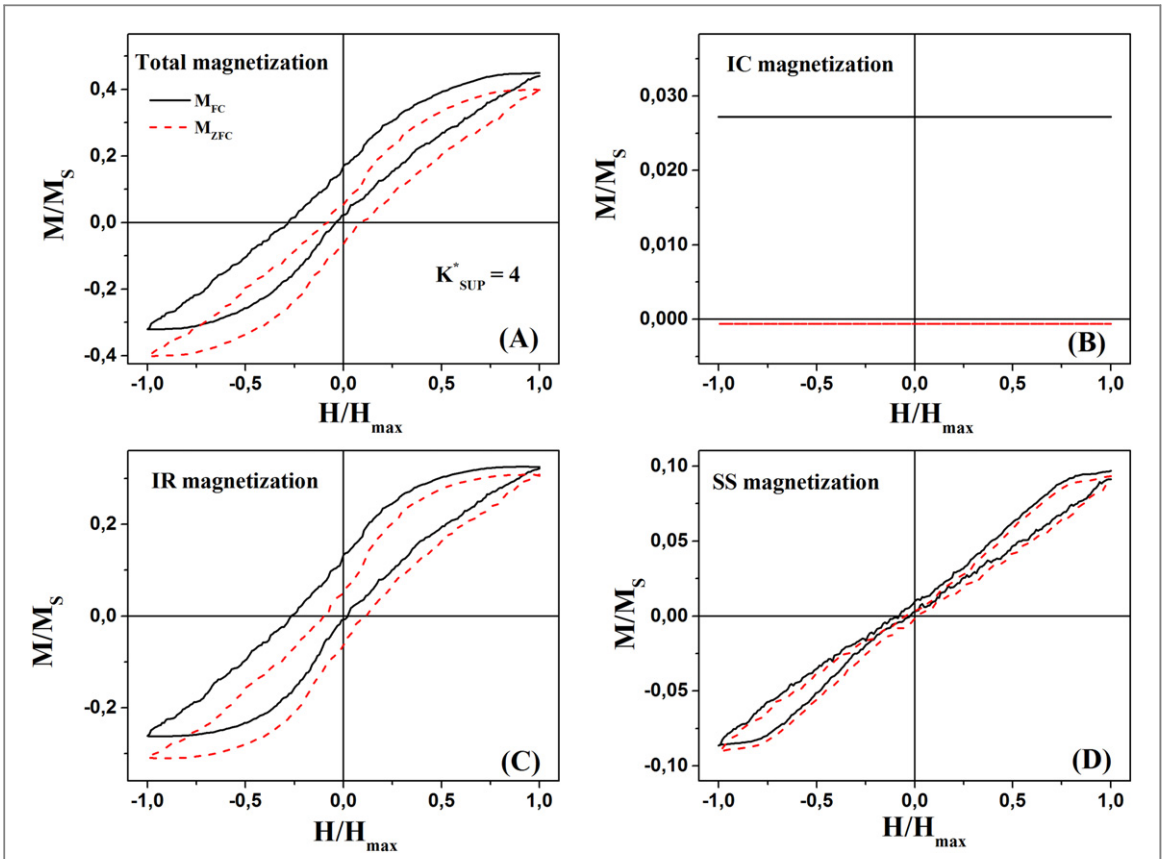

Figure 6. Simulated $M_{FC}(H)$ and $M_{ZFC}(H)$ hysteresis loops. (A) Total magnetization, (B) IC magnetization, (C) IR magnetization and (D) SS magnetization.

The numerical simulations were performed, according to the previously mentioned details, using the values of the physical parameters summarized in table 1, normalized to the surface anisotropy constant:

The asterisks on the parameter names reported in table 1 indicate that they are relative values.

Figure 6 shows the results of the $M_{FC}(H)$ and $M_{ZFC}(H)$ hysteresis loop simulation. The dashed red line corresponds to the M_{ZFC} and the full black one to the M_{FC}. The figure is divided into four panels: (A) total magnetization, (B) cluster magnetization, (C) IR spin magnetization and (D) surface magnetization contributions. The figure shows essentiality the same behavior observed in the experimental measurements (see figure 4). There is an exchange bias in the case of the M_{FC} protocol which is not observed on the M_{ZFC}. On the other hand, it is clearly seen that the cluster does not reverse its initial magnetization. Contrarily, the spins corresponding to the intermediate region, as well as to the surface, evidence the bias behavior. In addition, the simulation clearly shows the vertical displacement of the M_{FC} hysteresis loop with respect to the M_{ZFC} one. The simulation indicates that the IC spins are principally responsible for the exchange bias behavior. The large effective anisotropy field of these spins causes their magnetization and cannot be reversed by the effect of the external magnetic field sweeping. Then, the IC magnetization generates an effective internal magnetic field (through the exchange interaction) which originates the observed bias. The effect of this effective field propagates, by the antiferromagnetic exchange interaction, until the surface spins. Another important

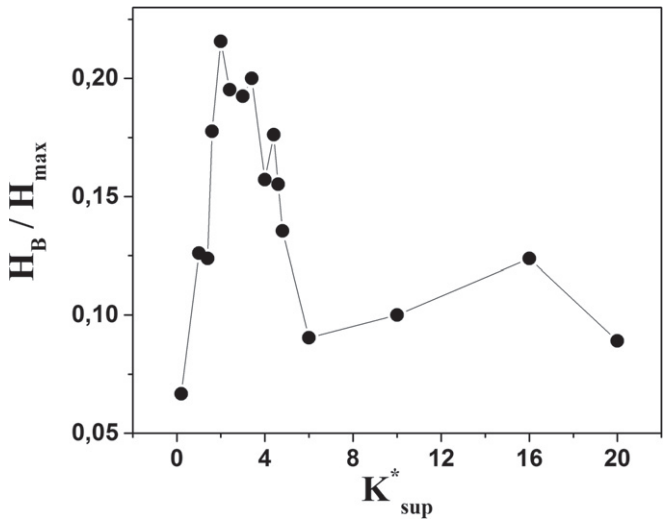

Figure 7. Exchange bias field calculated as a function of K^*_{sup} .

characteristic observed in the simulation compared with the experimental data of figure 4 is the particular elongated shape of the hysteresis loop, and also the small coercive field compared with the irreversibility field. We can see the similarity especially in the contribution of the surface spin's curve. This could indicate that, in our model, we have underestimated the spin's surface contribution.

In order to study the contribution of the surface anisotropy to the exchange bias behavior, we simulated hysteresis loops with different values of K^*_{sup} . In figure 7 we show the behavior of the exchange field as a function of K^*_{sup} . A clear maximum approximately at $K^*_{sup} = 4$ is observed. This result reveals that the surface anisotropy plays an important role in the magnetic behavior, particularly in the Exchange Bias phenomena. In order to understand the micromagnetic mechanisms that take place in the particle and the role of surface anisotropy in the observed shifted hysteresis cycle, we study the configurations of the magnetic spins. In figure 8 we show some snapshots of spin configurations obtained from the simulations. The figure consists of a cross section of the calculated spin configurations in the $x - z$ plane of the particle. The spin's length indicates the projection of each spin on the mentioned plane. The figure is divided into four panels, according to the value of the external magnetic field and the number of planes shown. The plane labeled 0 refers to a cross section in the middle of the particle, and the plane labeled 4 corresponds to a cross section at 4 planes of distance from the center. H_{max} and $-H_{max}$ labels indicate the maximum and minimum values of fields corresponding to these spin configurations. As figure 8 shows, the IC spins retain their magnetization unaltered in comparison to the data corresponding to H_{max} and $-H_{max}$ cases (panel (A) with (B), and (C) with (D)). The IR spins follow the external field orientation. This can be seen clearly in panels (C) and (D), which have a large number of IR spins.

The most interesting result is the behavior of the SS spins. These spins conserve their orientation almost unaltered when the field is changed. The effect of the external magnetic field on these spins is only a small tilt. This result indicates that the surface anisotropy generates a freeze [15–17] strong enough to 'delete' the effect of the external field. Then, if the system is cooled under an external applied field, it magnetizes the IC spins, and the effective field generated by this influences all of the particle spins, especially the surface ones. At very low temperatures the surface anisotropy becomes more relevant [14–17]. Then, the surface spins freeze their magnetic orientation according to the surface anisotropy and the effective field influence. In this way, the mechanism that originates the exchange bias is strengthened. However, if the anisotropy of the surface is very large, this could erase the effect of the internal field and decrease the shift in the hysteresis loop, as is observed in figure 7.

Based on the model used to explain the magnetic behavior observed for the HNS, we understand that the change in nanoparticle size should affect the bias phenomena. According to this model, changes in the size of internal clusters (which comprise the main contribution for the bias) affect the effective field generated by them. In addition, an increase/decrease in the overall particle size will decrease/increase the effect of surface magnetic anisotropy, which has an important role in reinforcing the effect of the internal field that generates the magnetic bias.

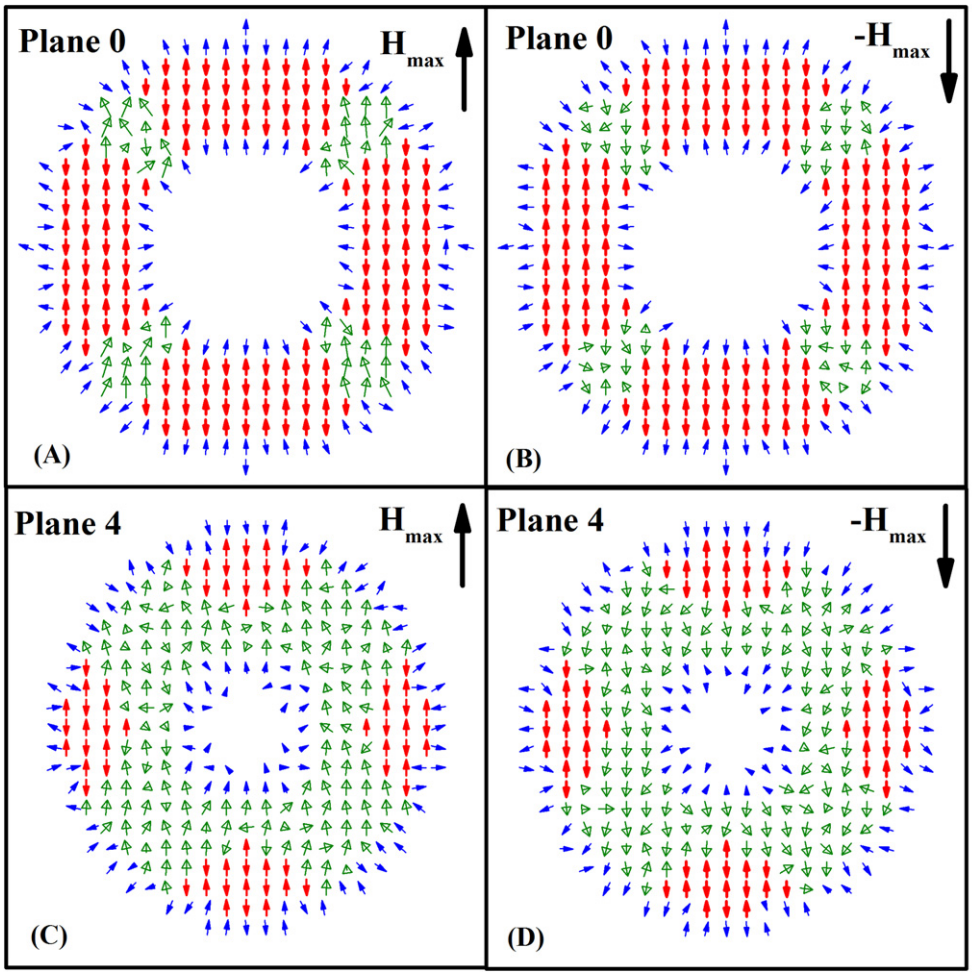

Figure 8. Cross section snapshot of spin configurations in the $x - z$ plane of the particle. (A) Plane 0 and H_{max}, (B) plane 0 and $-H_{max}$, (C) plane 4 and H_{max}, and (D) plane 4 and $-H_{max}$.

6. Conclusions

In this work, we report on the magnetic behavior of hollow nanospheres (HNS), which results from their unique structure and morphology. This system presents a complex internal magnetic structure, resulting in very unusual magnetic behavior. The magnetization measurements and in-field Mössbauer spectroscopy clearly show that the HNS has more than one magnetic phase despite its unique composition. The system has a magnetic ordering at low temperatures (below 20 K) and a magnetic frustration (∼11 K). However, the main result is the shift observed in the hysteresis loops when the system is cooled under an applied magnetic field.

We developed a micromagnetic model in order to reproduce the magnetic features of the HNS. This model not only reproduces the shift of the hysteresis loop but also allows us to understand the micromagnetic mechanism associated with the magnetic response of the system at very low temperature. The simulations indicate that the anomalous behavior starts on the internal clusters of the particle. The high value of the anisotropy field is hardening the reversion of their magnetization. This magnetic hardening generates an effective internal field that propagates to the entire particle through the exchange interaction. Our simulations also indicate that the surface anisotropy of the spins localized in both internal and external surfaces plays an important role in the observed features at low temperatures: it freezes the surface spin configurations, allowing them to keep the effect of the internal field generated on the internal magnetic clusters.

Acknowledgments

The authors are grateful to the Argentinean CONICET agency and to the Spanish agencies for their support.

References

[1] Kronmuller H 2007 *Handbook of Magnetism and Advanced Magnetic Materials* (New York: Wiley)
[2] Arruebo M, Fernández-Pacheco R, Ibarra M R and Santamaría J 2007 Magnetic nanoparticles for drug delivery *Nano Today* **2** 22–32
[3] Goya G F, Grazu V and Ibarra M R 2008 Magnetic nanoparticles for cancer therapy *Current Nanoscience* **4** 1–16
[4] Cao S-W, Zhu Y-J, Ma M-Y, Li L and Zhang L 2008 Hierarchically nanostructured magnetic hollow spheres of Fe3O4 and γ-Fe2O3: preparation and potential application in drug delivery *J. Phys. Chem.* C **112** 1851–6
[5] Iram M, Guo C, Guan Y, Ishfaq A and Liu H 2010 Adsorption and magnetic removal of neutral red dye from aqueous solution using Fe3O4 hollow nanospheres *J. Hazard. Mater.* **181** 1039–50
[6] Liu S, Xing R, Lu F, Rana R K and Zhu J 2009 One-pot template-free fabrication of hollow magnetite nanospheres and their application as potential drug carriers *J. Phys. Chem.* C **113** 21042–7
[7] Kodama R and Berkowitz A 1999 Atomic-scale magnetic modeling of oxide nanoparticles *Phys. Rev.* B **59** 6321–36
[8] Peng S and Sun S 2007 Synthesis and characterization of monodisperse hollow Fe3O4 nanoparticles *Angew. Chem. Int. Ed. Engl.* **46** 4155–8
[9] Martínez O B, Obradors X, Balcells L, Rouanet A and Monty C 1998 Low temperature surface spin-glass transition in g-Fe2O3 nanoparticles *Phys. Rev. Lett.* **80** 181–4
[10] Lima E *et al* 2009 Single-step chemical synthesis of ferrite hollow nanospheres *Nanotechnology* **20** 045606
[11] Hendriksen P V, Linderoth S, Oxborrow C A and Morup S 1994 Ultrafine maghemite particles: II. The spin-canting effect revisited *J. Phys.: Condens. Matter.* **6** 3091
[12] Néel M L 1949 Théorie du trainage magnétique des ferromagnétiques en grains fins avec applications aux terres cuites *Ann. Géophysique* **5** 99–136
[13] Brown W F 1963 Thermal fluctuations of a single-domain particle *Phys. Rev.* **130** 1677–86
[14] De Biasi E, Zysler R D, Ramos C A and Romero H 2002 Magnetization enhancement at low temperature due to surface ordering in Fe-Ni-B amorphous nanoparticles *Phys. B Condens. Matter* **320** 203–5
[15] De Biasi E, Ramos C, Zysler R and Romero H 2002 Large surface magnetic contribution in amorphous ferromagnetic nanoparticles *Phys. Rev.* B **65** 1–8
[16] De Biasi E, Zysler R D, Ramos C. a., Romero H and Fiorani D 2005 Surface anisotropy and surface-core interaction in Co-Ni-B and Fe-Ni-B dispersed amorphous nanoparticles *Phys. Rev. B–Condens. Matter Mater. Phys.* **71** 1–6
[17] Zysler R D, Romero H, Ramos C A, De Biasi E and Fiorani D 2003 Evidence of large surface effects in Co-Ni-B amorphous nanoparticles *J. Magn. Magn. Mater.* **266** 233–42
[18] Smit J and Wijn H P J 1959 *Ferrites: Physical Properties of Ferrimagnetic Oxides in Relation to their Technical Applications* (Eindhoven: Philips)
[19] Kittel C 2005 *Introduction to Solid State Physics* (New York: Wiley) p 325
[20] Fletcher R and Reeves C M 1964 Function minimization by conjugate gradients *Comput. J.* **7** 149–54
[21] Ginsburg T 1963 The conjugate gradient method *Numer. Math.* **5** 191–200